RESEARCH PAPER

PCCP
www.rsc.org/pccp

Characterization of adsorbed xenon in Zeolite-A, X, and Y by high-pressure ^{129}Xe NMR spectroscopy

Noriko Kato,[a] Takahiro Ueda,*[ab] Hironori Omi,[a] Keisuke Miyakubo[a] and Taro Eguchi[ab]

[a] *Department of Chemistry, Graduate School of Science, Osaka University, Toyonaka, Osaka, 560-0043, Japan*
[b] *The Museum of Osaka University, Toyonaka, Osaka, 560-0043, Japan. E-mail: ueda@museum.osaka-u.ac.jp; Fax: +81 6 6850 5785; Tel: +81 6 6850 5791*

Received 2nd August 2004, Accepted 7th October 2004
First published as an Advance Article on the web 22nd October 2004

The local structure of confined xenon in A-, X- and Y-type zeolites (molecular sieve 5A, 13X and zeolite NaY) was investigated by *in situ* high-pressure ^{129}Xe NMR spectroscopy. Xenon confined in dehydrated samples gives a resonance peak in the chemical shift range from 50 to 100 ppm at 0.1 MPa, and the chemical shift values increase as pressure increases. The pressure dependence of ^{129}Xe chemical shift on xenon confined in the micropores can be approximately described by the Langmuir adsorption model, resulting in the parameters being able to describe pore diameter, adsorption ability of the pore, and the local structure of the confined xenon atoms. Using these parameters, the pore structure, the mobility and the cluster size of xenon in the micropore are discussed for A- and X-type zeolites. Furthermore, the effect of pre-adsorbed water and the binder for pellet preparation on the pore structure is also examined. In the Y-zeolite, a chemical exchange of xenon between the outside and inside of the micropores was observed above 0.75 MPa. Spectral simulation assuming a simple two-site exchange model revealed the exchange rate constant and the population ratio of xenon in the exchange between the outside and the inside the micropores. The exchange of xenon is optimum around the supercritical point of the bulk xenon ($\sim$6 MPa), and decreases above 6 MPa, and this originates from the cooperative phenomenon in the supercritical fluid.

1. Introduction

Zeolites are crystalline porous aluminosilicates including alkali and/or alkaline earth metals, with the chemical composition of $M_{x/n}\cdot[(AlO_2)_x(SiO_2)_y]\cdot wH_2O$. These compounds exhibit interesting properties such as molecular sieve ability and catalysis.[1] These properties can be modified by chemical treatment such as ion exchange and/or de-alumination. Many researchers have investigated these materials at the scientific and engineering points of view,[2–4] and it has been found that the adsorption behavior, reactivity, and molecular sieve ability of zeolites are closely related to the framework, porous structure, and intermolecular interactions between the pore wall and the adsorbed molecule, as well as between the adsorbed molecules. In addition, adsorbed water present in the micropores and the formation of macro- and mesopores due to the aggregation of fine particles of zeolites, will also affect the adsorption behavior of the zeolites. The adsorbed water decreases the volume of the micropore to less than 0.5 nm, which is a so-called ''ultramicropore'', and screens the guest molecules from the pore wall, affecting the functional properties of zeolites such as catalysis, the molecular sieve and reactivity. Furthermore, the adsorbent products consist of fine particles of synthetic zeolite with a μm diameter order, which are bound by binder agents such as clay, phosphates, and glass with a low melting point to prepare the pellets and/or beads for easy handling. The addition of binder agents to form pellets leads to extra pores of 1–50 nm. These meso- and macropores increases in the amount of adsorbate at the large value of the relative pressure and play an important role in the process of the diffusion of the adsorbates such as molecular diffusion and Knudsen diffusion.[65]

^{129}Xe NMR is an important tool in the study of ultra-micro, micro-, meso-, and macropores. Xenon-129 NMR spectroscopy has been developed to study the structure and topology of internal voids, adsorption sites, and intermolecular interactions in porous materials, since the potential of xenon-129 as a probe for the inner space of materials was proposed by Ito and Frassard[5] in 1980. Recently, this smart methodology has been widely used in the characterization of porous materials as a modern and sophisticated technique of porosimetry,[5–9] and the local structure of materials such as zeolites,[5,10–15] glass,[16] fullerenes,[17] carbon nanotubes,[18] polymers,[19–22] and clathrate compounds,[23–26] liquid crystals,[27–29] some organic solvents,[9,30] and proteins in solution[30–32] have been investigated. In the past decade, hyperpolarized (HP) xenon NMR techniques have been developed to enhance the sensitivity of ^{129}Xe NMR.[33,34]

However, to obtain information from ultramicro- and/or meso- and macropores using xenon as a probe, it is necessary to confine xenon in ultra-micropores of the same size as xenon, and/or to slow down the exchange between xenon adsorbed in meso- and macropores and the bulk. It is difficult to achieve this situation under ambient conditions, and high-pressure conditions offer a solution. We recently described a conventional and newly designed *in situ* variable pressure NMR probe, allowing studies with pressures up to 20 MPa,[22] and it has been applied in the study of xenon–wall interactions in the free volume of polymers,[35] the intermolecular interaction of xenon confined in 1D-nanochannels,[36,37] and the supercritical phenomenon of xenon in mesoporous silica.[38] Furthermore, Brunner *et al.* have reported the pressure dependence of ^{129}Xe chemical shift in the supercritical state up to a pressure of about 70 MPa using a high-pressure cell made from a sapphire tube.[39] This high pressure condition is expected to offer new insights into xenon–wall and xenon–xenon interactions for xenon confined in nanospaces, as well as the dynamic behavior of xenon in nanospaces.

In this study, we applied the high-pressure ^{129}Xe NMR technique to some typical zeolites: molecular sieve 5A, 13X, and zeolite NaY. Molecular sieve 5A has a type-A framework

DOI: 10.1039/b411798k

(LTA) with the chemical composition of $(Ca_{4.8}, Na_{2.4})[(AlO_2)_{12}(SiO_2)_{12}] \cdot wH_2O$, with the unit cell having a lattice symmetry of $Pm3m$, a lattice constant of $a_0 = 1.24 \pm 0.001$ nm, and a maximum diameter of 1.14 nm for the super cage which is linked each other by the window with a diameter of about 0.5 nm.[40–42] In contrast, molecular sieve 13X and zeolite NaY have a faujasite X- and Y- type framework (FAU) with the chemical composition of $Na_x[(AlO_2)_x(SiO_2)_{192-x}] \cdot wH_2O$, respectively, with the unit cell having a lattice symmetry of $Fd3m$, a lattice constant of $a_0 = 2.49 \pm 0.01$ nm and a maximum diameter of 1.37 nm for the super cage which is linked each other by the window with a diameter of 0.74 nm.[42,43] We have investigated the adsorption behavior of xenon on these zeolites using high-pressure ^{129}Xe NMR spectroscopy to clarify the influence of the framework, the adsorbed water and the binder agents on the adsorption behavior of xenon under high-pressure conditions.

2. Experimental

Chemicals

Powdered samples of molecular sieve 5A, 13X, and zeolites NaY were purchased from Aldrich Co. Ltd. Pellets of molecular sieves were purchased from Nakarai Co. Ltd. Sample dehydration was achieved by heating at 400 °C under reduced pressure ($P < 2 \times 10^{-2}$ Torr) for 3–24 h after roughly drying the specimens at ambient temperature under reduced pressure for 12 h. All the specimens were characterized by thermogravimetric analysis (TG), nitrogen adsorption isotherm, ^{29}Si MAS NMR spectrum, and powder X-ray diffraction (XRD) to confirm the amount of adsorbed water, the pore volume and the specific surfaces, and the ratio of SiO_2 to AlO_2 (Si/Al) in the framework.

Thermogravimetric analysis (TG)

TG analysis was carried out using SEIKO I SSC-5020M II TG/DTA 200-type thermal analysis equipment. TG diagrams were recorded at a heating rate of 10 K min^{-1} up to 600 °C under nitrogen gas flow at a rate of 50 ml min^{-1}. α-Alumina, α-Al_2O_3, was used as a reference sample.

N_2 adsorption isotherm measurements

Nitrogen adsorption isotherms were measured using Shimazu Gemini 2375 automatic specific surface measuring apparatus in the relative pressure range P/P_0 from 0.001 to 0.95.

^{29}Si MAS NMR measurements

^{29}Si magic-angle spinning (MAS) NMR spectra were measured using a Bruker DSX-200 spectrometer with a Larmor frequency of 39.7 MHz. Free-induction decay (FID) signals were recorded in a single pulse experiment using a pulse delay of 80 s, and π/2-pulse of 8 μs, under 4 kHz of MAS rate at room temperature. The chemical shift was referenced by tetramethylsilane (TMS) as an external standard.

Powder X-ray diffraction (XRD) measurements

XRD measurements were carried out using a Rigaku Rotaflex Rint 2000 diffractometer on HP 9000 S712/60 system from 3° to 60° in 2θ. The scan rate was 1.00° min^{-1}, and the increment step was 0.01°.

High-pressure ^{129}Xe NMR measurements

High-pressure ^{129}Xe NMR measurements were carried out using a Bruker MSL-200 spectrometer with a Larmor frequency of 55.6 MHz, in which a home-built *in situ* pressure variable NMR probe[22] was installed. The powdered or pellet samples were packed into a glass tube of 5 mmϕ, with both ends capped with glass wool, and the tube and samples were placed in a pressure-resistant NMR cell made from ZrO_2. The prepared NMR cell was then mounted onto the high-pressure NMR probe. The FID signals were recorded in a single-pulse experiment with a pulse delay of 5 s, π/2-pulse of 3 μs and accumulation of 8-8192, depending on the signal-to-noise ratio, over a pressure range of 0.01 to 10 MPa at 298 K. ^{129}Xe chemical shift was referenced by a signal from xenon gas at zero density. Temperature and pressure were controlled within the experimental error of ±0.5 K and 10% in MPa, respectively.

3. Results

3.1 Characterization of samples using TG, N_2 isotherm, and ^{29}Si MAS NMR

Thermogravimetric (TG) measurement of pre-heated samples up to 600 °C suggests that water adsorbed in the samples was removed by heating above 400 °C. The amount of adsorbed water, defined by the ratio of the weight of water to the weight of the dehydrated zeolites, was determined from the weight loss as follows; 41% for molecular sieve 5A, 100% for molecular sieve 13X and 163% for Zeolite NaY.

After dehydration of the samples by heating at 400 °C under reduced pressure, the N_2 adsorption isotherm was measured to characterize the amount of nitrogen at the maximum adsorption (W_{sat}), the specific surface area (S_{total}), the pore volume (V_{pore}), the external surface area (S_{ex}), and the internal specific surface area (S_{in}). These samples give the typical I-type adsorption isotherm according to the IUPAC classification.[44,45] The pore volume, external and internal surface areas are given by *t*-plot analysis.[46] The parameters determined are listed in Table 1.

^{29}Si magic angle spinning (MAS) NMR spectrum gives the atomic ratio of Si to Al, Si/Al for each sample as listed in Table 1.[47–50] According to the results of TG and ^{29}Si MAS NMR, we can determine the chemical composition of each sample: $(Ca_{4.8}, Na_{2.4})[(AlO_2)_{12}(SiO_2)_{12}] \cdot (\sim 39)H_2O$ for molecular sieve 5A, $Na_{84}[(AlO_2)_{84}(SiO_2)_{108}] \cdot (\sim 750)H_2O$ for molecular sieve 13X, and $Na_{52}[(AlO_2)_{52}(SiO_2)_{140}] \cdot (\sim 1200)H_2O$ for Zeolite NaY.

3.2 ^{129}Xe NMR spectrum for dehydrated powder samples

Figs. 1(a)–(c) show the pressure dependence of the ^{129}Xe NMR spectrum in dehydrated powder samples of molecular sieve 5A, 13X and zeolite NaY, respectively. The pressure dependence of

Table 1 Characterization of micropores and Si/Al in molecular sieve 5A, 13X and Zeolite NaY determined from N_2 isotherm adsorption and ^{29}Si MAS NMR measurements

Sample	W_{sat}/cm^3 g^{-1}	S_{total}/m^2 g^{-1}	S_{in}/m^2 g^{-1}	S_{ex}/m^2 g^{-1}	V_{pore}/cm^3 g^{-1}	Si/Al
5A	176	760	751	9.20	0.263	1
13X	215	925	910	14.3	0.317	1.3
NaY	225	951	937	14.6	0.328	2.7

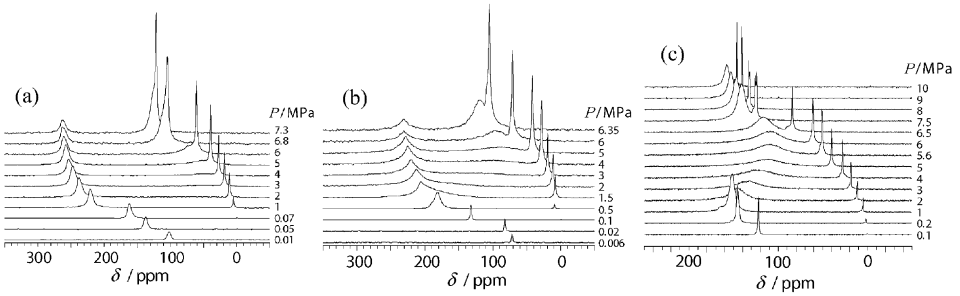

Fig. 1 Pressure dependence of ^{129}Xe NMR spectra of molecular sieve 5A (a), 13X (b), and NaY powder (c) specimens. All samples were dehydrated for 3 h in a vacuum at 673 K before measurement.

the chemical shift values for each resonance line is shown in Fig. 2. In each sample, the spectrum at 0.1 MPa mainly consists of two dominant peaks; one near 0 ppm and other at the chemical shift range from 50 to 100 ppm.

The resonance line near 0 ppm comes from bulk free xenon gas coexisting on the powder sample. The chemical shift of this resonance line agreed with that for pure bulk xenon gas within the experimental error, suggesting that the observed peak for bulk free xenon is not affected by the chemical exchange with xenon adsorbed in the micropores.

On the other hand, the peak appearing in the lower field corresponds to xenon adsorbed in the micropore, and shifts toward the lower field side as pressure increases. The δ-value, which is extrapolated to zero pressure using the data below 0.1 MPa, gives 90 ppm for molecular sieve 5A, 65 ppm for 13X and 52 ppm for zeolite NaY, and increases rapidly as pressure increases to 1 MPa. For molecular sieve 5A and 13X, it reaches 260 ppm and 230 ppm at 6 MPa, respectively. In addition to these two peaks, the extra peak appears at the chemical shift range 20–30 ppm higher than that of bulk-free xenon above 5 MPa. This peak originates from partial components of xenon contributing to the chemical exchange between the inside and outside of the micropore.[11,51]

In contrast, in zeolite NaY, the resonance line shifts again toward the higher field above 1 MPa with the line broadening, and the δ-value for xenon in the micropore shows the minimum level of 110 ppm at 6 MPa. Above 6 MPa, the resonance line shifts again to the low field with narrowing of the lines. Furthermore, under 4 MPa pressure, the resonance line at 306 K (FWHM $\sim$70 ppm) becomes narrower than that at 298 K (FWHM $\sim$100 ppm) as shown in Fig. 3. This anomalous pressure dependence is caused by the influence of the rapid chemical exchange of xenon between the inside and outside of the micropores.

3.3 ^{129}Xe NMR spectrum for hydrated powder samples

Figs. 4(a) and 4(b) show the pressure dependence on the ^{129}Xe NMR spectrum for the powder sample of molecular sieve 5A and 13X before dehydration. The chemical shift for xenon in the micropore entirely shifts the lower field compared to the dehydrated samples. Fig. 5 shows the pressure dependence of the chemical shift value for each sample, in which the δ-value extrapolating to zero pressure is evaluated as 127 ppm for molecular sieve 5A, and 160 ppm for 13X. These values are 37 ppm and 95 ppm greater than for each dehydrated sample. The chemical shift value increases 100 ppm for 5A and 35 ppm for 13X as pressure increases up to 6 MPa. In these samples, the extra broad peak, which appears at 20–30 ppm higher than the peak of free xenon in the dehydrated samples above 5 MPa (See Fig. 1(a) and 1(b)), was not observed.

3.4 ^{129}Xe NMR spectrum for pellet samples

Figs. 6(a)–(d) show the pressure dependence of ^{129}Xe NMR spectra of xenon adsorbed in the pellet samples of molecular sieve 5A and 13X. In molecular sieve 5A, the pressure dependence of ^{129}Xe NMR spectra is similar in both the hydrated (Fig. 6(a)) and dehydrated (Fig. 6(b)) pellet samples. The extra resonance peak, which appears above 4 MPa in the dehydrated powder sample in Fig. 1(a), was also observed in the pellet dehydrated sample. It is considered that the existence of some additional porous structure such as micro-, meso- and macropores, which is caused by binder agents, is not clear in molecular sieve 5A. On the other hand, in molecular sieve 13X, the resonance peak from xenon in the micropore is split

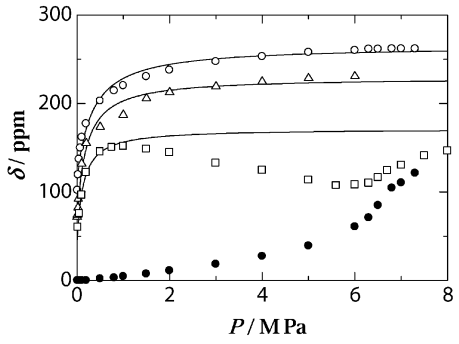

Fig. 2 Pressure dependence of ^{129}Xe NMR chemical shift values of xenon confined in molecular sieve 5A (○), 13X (△), and NaY (□) powder specimens. All samples were dehydrated for 3 h in a vacuum at 673 K. The filled circle (●) shows the pressure dependence of the chemical shift values of free xenon gas co-existing with the samples, which coincides with those for pure bulk-xenon gas.

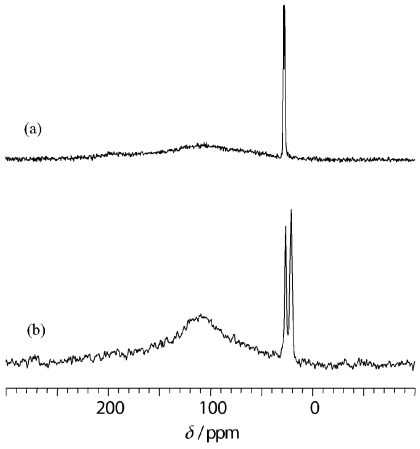

Fig. 3 ^{129}Xe NMR spectra of zeolite NaY at $T = 298$ K (a), and 306 K (b) under the pressure of 4 MPa. The peak for free xenon gas split into two peaks at 306 K. This will be caused by the inhomogeneity of temperature in the high pressure NMR cell. Air flow from the underneath of the cell is heating the lower side of the cell, resulting in a temperature difference between the upper side and lower side of the cell.

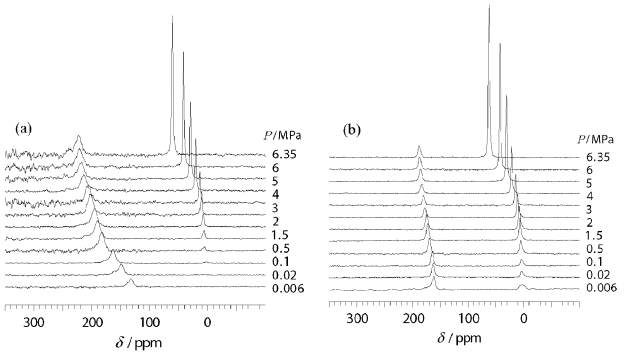

Fig. 4 Pressure dependence of ^{129}Xe NMR spectra of the partially hydrated powder specimens: molecular sieve 5A (a) and 13X (b).

into two peaks in the pellet sample. It is considered that there are two types of micropores in the pellet samples. The intensity of these peaks depends on the presence of adsorbed water. In the partially hydrated sample (Fig. 6(c)), the peak in the higher field is dominant, whereas in the dehydrated sample (Fig. 6(d)), the intensity of these peaks is reversed. This suggests that micropores corresponding to these two peaks have different affinity for water adsorption, that is, the micropore with a resonance peak in the lowest field can adsorb water easier than that with a resonance peak in the higher field. As pressure increases, the line width of both peaks broadens, but these peaks did not coalesce.

4. Discussion

4.1 Pressure dependence of ^{129}Xe chemical shift

The pressure dependence of the ^{129}Xe chemical shift of xenon confined to micropores is similar to the xenon adsorption isotherm classified in type-I by IUPAC,[44,45] suggesting that the adsorption of xenon is accelerated in low pressure regions due to the deep potential, which is emphasized by the micropore field. When the contribution of local magnetic fields in the pore to the chemical shift is quite small and there are no strong adsorption sites for xenon, the ^{129}Xe chemical shift for xenon adsorbed in the pore is described by

$$\delta = \delta_S + \delta_{Xe} + \delta_E \qquad (1)$$

where δ_S is the interaction between xenon and the wall of the pore, and δ_{Xe} is the contribution of Xe–Xe interaction.[10,52] The second term of the right hand side of eqn. (1) is assumed to be proportional to the density of xenon in the pore, and is approximated to be $\delta_{Xe} = \delta_{Xe\text{–}Xe}\rho$. Therefore, the plateau observed on the pressure dependence of ^{129}Xe chemical shift

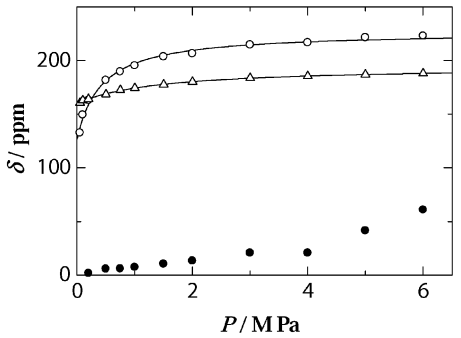

Fig. 5 Pressure dependence of ^{129}Xe NMR chemical shift values of xenon confined in the partially hydrated molecular sieve 5A (○) and 13X (△) powder specimens. The filled circle (●) shows the pressure dependence of the chemical shift values of free xenon gas co-existing with the samples, which coincides with those for the pure bulk-xenon gas.

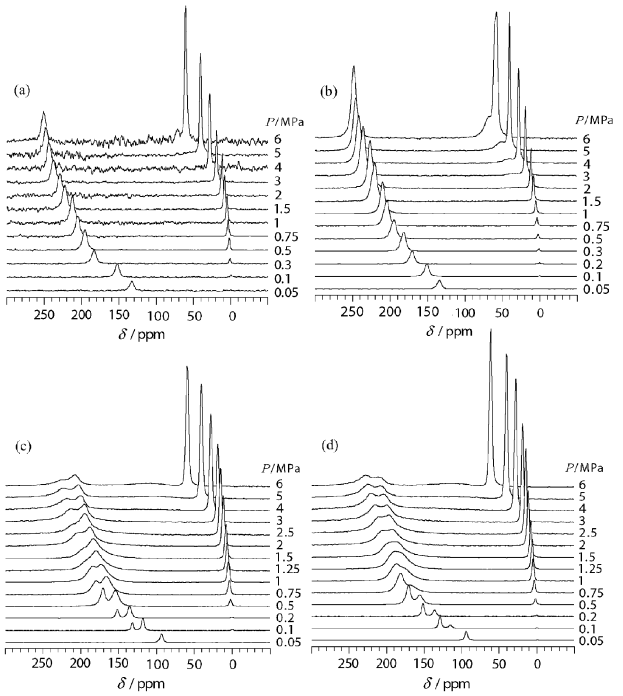

Fig. 6 Pressure dependence of ^{129}Xe NMR spectra of the pellet specimens of molecular sieve 5A and 13X; partially hydrated sample of 5A (a), dehydrated sample of 5A (b), partially hydrated sample of 13X (c) and dehydrated sample of 13X (d).

in high-pressure regions indicates that the adsorption of xenon in the micropores of molecular sieve 5A and 13X has reached saturation. The third term is contribution of local electric field caused by charge center such as Ca^{2+}. This term will contribute the chemical shift in molecular sieve 5A containing Ca^{2+}. Although the adsorption amount of xenon in molecular sieve 5A and 13X in high-pressure regions up to 10 MPa enables the discussion of the density dependence of the chemical shift, the xenon adsorption isotherm in these systems is unknown. The appropriate assumption of the adsorption of xenon in high-pressure regions leads to the pressure dependence of xenon density in micropores. In this study, this is assumed by the Langmuir equation, because the physisorption due to micropore filling (type-I) can be qualitatively approximated by the Langmuir equation.[53,54] The surface coverage of xenon in micropores, θ, is defined by the density ratio at equilibrium pressure to the density when the adsorption is saturated, $\rho(P)/\rho(\infty)$. In Langmuir-type adsorption behavior, the coverage is given by

$$\theta = \frac{KP}{1 + KP} \qquad (2)$$

where K is the ratio of the rate constant for adsorption to desorption. Furthermore, the change in the chemical shift value between 0 MPa and infinite pressure is represented by $\Delta\delta_{Xe\text{–}Xe} = \delta(\infty) - \delta_S$. Using these relationships, the ^{129}Xe chemical shift at pressure, P, is represented by

$$\delta = \delta_S + \Delta\delta_{Xe\text{–}Xe}\frac{KP}{1 + KP}. \qquad (3)$$

We can discuss the adsorption behavior of xenon using the parameters, δ_S, $\Delta\delta_{Xe\text{–}Xe}$, and K, obtained from the pressure dependence of ^{129}Xe chemical shift value. In particular, parameters such as $\Delta\delta_{Xe\text{–}Xe}$ and K, which relate to xenon–xenon interaction in the adsorption process of xenon, are given as high-pressure ^{129}Xe NMR measurements, in addition to δ_S which can be determined from conventional ^{129}Xe NMR measurements covering only the low-equilibrium pressure range.[10–15] The analysis of the pressure dependence of ^{129}Xe

chemical shift using eqn. (3) leads to three kinds of parameters for each sample as listed in Table 2. In NaY zeolite, the analysis was carried out using chemical shift data below 0.75 MPa.

4.2 Pore size from δ_S

δ_S reflects the interaction between xenon and pore walls. Fraissard *et al*. assumed that δ_S is given by the average value between the chemical shifts of xenon on the wall, δ_a, and in free space, δ_V, for de-aluminated zeolites and zeolites containing only Na^+ as a cation as follows:[55]

$$\delta_S = \frac{n_a\delta_a + n_v\delta_v}{n_a + n_v} \quad (4)$$

where δ_V depends on the volume of free space in the pores. On the basis of this assumption,[56] there is a relation between δ_S and the mean free path, l, of xenon in the pore as represented by

$$\delta_S = 243\frac{0.2054}{0.2054 + l}\ . \quad (5)$$

This equation suggests a linear relation between the reciprocal value of δ_S and the pore size. Assuming the shape of the pore as a sphere and cylinder, the mean free path of xenon is given by $l = (D_S - D_{Xe})/2$ and $l = (D_C - D_{Xe})$, respectively, using the pore diameter, D_S and D_C for spherical and cylindrical pores and the van der Waals diameter of xenon, D_{Xe}. According to these equations, the following relations are derived between δ_S and D_C and/or D_S:[56]

$$D_S = \frac{99.8}{\delta_S} + 0.029, \quad (6a)$$

$$D_C = \frac{49.9}{\delta_S} + 0.235. \quad (6b)$$

These equations have previously been proposed to explain the relation between the chemical shift and the free space in micropores. Although it has recently been attempted to elucidate the chemical shift of xenon in the pores using *ab initio* MO calculations on the basis of xenon–wall as well as xenon–xenon interactions,[57] it is convenient to describe the relation between δ_s and the pore size of zeolites. Using these equations, we can evaluate the pore diameter of molecular sieve 5A and 13X for hydrated and dehydrated samples, and dehydrated zeolite NaY as listed in Table 2. In molecular sieve 5A, δ_E also contributes to δ at zero pressure. Although the effect of δ_E on δ will leads to overestimation of δ_S, δ at zero pressure, which corresponds to $\delta_S + \delta_E$, enables us to roughly estimate the pore diameter.

The pore diameter evaluated from the crystal structure is 1.14 nm for molecular sieve 5A and 1.37 nm for molecular sieve 13X and zeolite NaY. Comparing the pore size from δ_S assuming the spherical and cylindrical shape to that one, the spherical and cylindrical pore model seems to be valid for molecular sieve 5A and zeolite NaY, respectively. For molecular sieve 13X, the pore size from the crystal structure is the intermediate value of the spherical and cylindrical pore model. This aspect may concern the mobility of adsorbed xenon in the pore. In molecular sieve 5A, xenon is strongly adsorbed in the super cage, resulting in the long residence time of xenon in the cage. Consequently, the adsorbed xenon assumes a spherical shape in the occupying space. As the rate of translational motion of xenon increases in the pore, the residence time of the adsorbed xenon in the super cage decreases and xenon translating from the super cage to others assumes a cylindrical shape in the occupying space. The effective shape of the pore describing δ_S implies that the mobility of xenon decreases in the order; NaY > 13X > 5A.

4.3 Influence of adsorbed water on the xenon adsorption

The analysis of the pressure dependence of ^{129}Xe chemical shift in the hydrated sample for molecular sieves gives the parameters, δ_S, $\Delta\delta_{Xe-Xe}$, and K as listed in Table 2. In fact, the influence of the adsorbed water on the xenon chemical shift was already examined in NaY.[66] In NaY, both δ_{wall} and δ_1, which correspond to δ_S and δ_{Xe} in this paper, were affected by the amount of water. The effect of the presence of water on the xenon environments is different between the adsorption and desorption processes of water: Adsorption of water leads to inhomogeneous distribution of xenon environments, whereas desorption leads to uniform one. In molecular sieve 5A and 13X, xenon environment seems to be uniform because of the single and symmetric peak for confined xenon (See Fig. 4). This implies that the samples used in this study are in the partially dehydrated condition.

The δ_S values in the hydrated samples are larger than the correspondence values for the dehydrated samples. Since the reciprocal value of δ_S is proportional to the pore size, which depends on the pore model, this aspect suggests that the pore size felt by adsorbed xenon decreases due to water adsorption in the hydrated samples. In molecular sieve 5A, the decreased pore diameter for the spherical pore shape is 0.30 nm, which corresponds to a 0.5 monolayer of water with 0.27 nm cross-section based on the van der Waals diameter of O- and H-atoms. On the other hand, in molecular sieve 13X, the decreased pore diameter is 0.95 nm for the spherical pore and 0.45 nm for the cylindrical pore and the average of these values is 0.70 nm, suggesting that about 1.3 molecular layers of water are formed on the wall, that is, the amount of adsorbed water in 13X is 2.6 times greater than that in 5A. This is consistent with the amount of water adsorbed in the pretreated samples determined by TG measurements, in which the amount of adsorbed water in 13X is 2.3 times greater than that in 5A; 41 wt.% for 5A and 100 wt.% for 13X. The δ_{wall} value in NaY changes from 58 ppm for completely dehydrated sample to 158 ppm for the sample containing 85% of the saturated water content.[66] This change is similar to that in molecular sieve 13X.

The $\Delta\delta_{Xe-Xe}$ value is related to the local density of xenon in the pore when the micropore is saturated by xenon. In addition, at low density where the additivity of the ^{129}Xe chemical shift value is valid for the amount of xenon occupying the

Table 2 The characteristic parameters of Xe adsorption in the samples determined by the pressure dependence of ^{129}Xe chemical shift value on the basis of the Langmuir adsorption model, and the estimated pore diameters from δ_S by assuming spherical (D_S) and cylindrical (D_C) spaces

Sample	Treatment	δ_S/ppm	$\Delta\delta_{Xe-Xe}$/ppm	K/MPa^{-1}	D_S/nm	D_C/nm
5A	Dehydrated	90	170	5.5	1.1	0.79
	Non-treated	127	100	2.4	0.80	0.63
13X	Dehydrated	65	167	4.3	1.6	1.0
	Non-treated	160	35	0.72	0.65	0.55
NaY	Dehydrated	52	121	6.0	1.9	1.2

nearest neighbors, this value will approximately reflect the number of surrounding xenon atoms for a xenon atom. According to the discussion on the additivity of the ^{129}Xe chemical shift to gaseous xenon adsorbed in the α-cage of zeolite A by Jameson *et al.*,[58] the additivity is valid for the cluster sizes up to Xe_6 and the shift value increases to about 22 ppm on average by the addition of one xenon atom. For Xe_7 and Xe_8 clusters, the chemical shift increases by about 45 ppm and 44 ppm when a xenon atom is added to the cluster, because the increase in cluster size leads to a large contribution of the chemical shielding at a shorter interatomic distance. On the basis of this discussion, the $\Delta\delta_{Xe-Xe}$ value for a dehydrated sample for 5A and 13X suggests the formation of a Xe_n cluster with an average size of $n = 7$, whereas for the hydrated sample, the decrease in $\Delta\delta_{Xe-Xe}$ value leads to the average size of cluster Xe_6 for 5A and of Xe_3 for 13X. In addition, the hydration also decreases in K value, implying that the hydrophobic interaction between xenon and the wall consisting of SiO_2 and/or AlO_2 is more efficient than the xenon–water interaction.

4.4 Pore structure in pellet samples

Figs. 6(c) and 6(d) suggest that there is a space larger than the original micropore of the zeolites in molecular sieve 13X. This may be the effect of the binder agents used in preparing the pellets, that is, relatively large micropores and/or mesopores are formed in the interspace between microcrystallites. This effect is clear in molecular sieve 13X. Above 0.1 MPa, the extra resonance line appears at a chemical shift 15 ppm smaller than the chemical shift corresponding to xenon in the original micropore. Since the potential well for adsorption due to the pores is inversely proportional to the pore size,[54,59] the larger the micropore diameter, the smaller the chemical shift value. Therefore, the extra peak will correspond to xenon adsorbed in the micropores and/or mesopores formed by the process of fine particle binding. In addition, the broadening of the line width of the peak for xenon in larger sized pores than the original, indicates the exchange of xenon between these pores, but these peaks did not coalesce. This implies that the exchange of xenon between these sites is very slow compared with the frequency separation of about 800 Hz (~15 ppm).

For xenon adsorbed in the extra pores, the spectrum depends on the hydration condition of the sample. In the hydrated sample, the intensity of the peak from xenon in the original micropore is smaller than that in the extra-large pores. In contrast, in the dehydrated sample, the intensities of these peaks are reversed. This aspect suggests that the hydration water is adsorbed in the original micropore formed by the zeolite frameworks more efficiently than the extra-large pores formed in the intercrystallites. This is caused by the deeper potential depth in the original micropore of 13X framework formed by the pore wall. For molecular sieve 5A, this effect cannot be observed.

4.5 Chemical exchange of xenon in NaY zeolite

In NaY, the pressure dependence of the resonance line with line broadening is related to the chemical exchange of xenon between the outside and inside of pores. The change in the chemical shift at pressures above 1 MPa in Fig. 2 is quite different from those for molecular sieve 5A and 13X. As an initial approximation, the pressure dependence of the chemical shift in pressure regions from 0.02 to 0.75 MPa is analyzed by the Langmuir adsorption model, because in this region, the pressure dependence is similar to those for the other two samples. The analysis leads to the following parameters: δ_S = 52 ppm, $\Delta\delta_{Xe-Xe}$ = 121 ppm, and K = 6.0 MPa^{-1}. In the pressure region higher than 0.75 MPa, the Langmuir model cannot explain the pressure dependence of the chemical shift. In contrast, part of the xenon gas co-existing with adsorbed xenon in the pore gives rise to a resonance line which coincides with the resonance for pure bulk xenon gas under the same conditions, implying that the effect of the chemical exchange of xenon is rarely affected in the observed part as free xenon gas in the spectrum.

When the chemical exchange of xenon between the outside and inside of the pore occurs with the exchange rate faster than the frequency separation between two resonance peaks in relation to the exchange, a resultant resonance peak appears at a frequency given by the weighted average of these two resonance frequencies. The line width of the averaged resonance line is efficiently affected by the exchange rate and the population of xenon in both sites. Thus, the temperature dependence of the spectrum in Fig. 3 strongly suggests the existence of the chemical exchange of xenon.

Using the simple two-site exchange model,[60] we then analyzed the pressure dependence of the spectrum to evaluate the exchange rate for xenon between the outside and inside of the pores. Two sites for xenon, bulk-xenon gas and adsorbed xenon in the pore, are denoted by A and B, respectively, where the population of each site is p_A and p_B and the exchange rate constant from A to B site is k_A and that from B to A site is k_B. According to the principal of the detailed balance, $p_A k_A = p_B k_B$ is satisfied. The residence time of xenon in each site is $\tau_A = {k_A}^{-1}$ and $\tau_B = {k_B}^{-1}$. In the slow exchange limit, the line width of the Lorentzian line shape function is then given as follows: $\Delta\nu_A = (\pi T_{2A})^{-1} + (\pi\tau_A)^{-1}$ for site A and $\Delta\nu_B = (\pi T_{2B})^{-1} + (\pi\tau_B)^{-1}$ for site B, where T_{2A} and T_{2B} are the transverse relaxation times for each original resonance peak of xenon at sites A and B, respectively. As the exchange rate increases, the line width also increases. They are given by the inverse of the line width at half maximum for each resonance peak, when the chemical exchange is negligible. In the fast exchange limit, the resonance line appears at a frequency given by the weighted average between the frequencies of site A and B as follows:

$$\nu = p_A\nu_A + p_B\nu_B \tag{7}$$

and the line width is given by

$$\Delta\nu = \frac{p_A T_{2A} + p_B T_{2B}}{\pi T_{2A} T_{2B}} + \frac{4\pi p_A p_B (\nu_A - \nu_B)^2}{k_A + k_B}. \tag{8}$$

The eqn. (8) indicates that the resonance frequency and the line width strongly depend on the population of xenon in each site as well as the exchange rates. Spectrum analysis was carried out using the GAMMA simulation program.[61] The variables in the simulation are the ratio of the population of xenon in the pore to that for bulk xenon, and the exchange rate constant between these two sites. In simulating the spectrum, we used various assumptions for the following points: (i) The original peak position (ν_B) for xenon adsorbed above 0.75 MPa is assumed to be given by the curve using the Langmuir model for the chemical shift value below 0.75 MPa. (ii) The line width (T_{2A} and T_{2B}) for each original peak without the effect of the chemical exchange is assumed to be identical to that of the resonance peak for pure bulk xenon (*ca.* 50 Hz). (iii) For bulk xenon gas, the chemical shift values for pure bulk xenon gas are used as the original resonance peak position (ν_A) at the corresponding pressure. The observed and simulated spectra are shown in Fig. 7(a) and 7(b), which focus on the chemical shift range from 40 to 200 ppm. The simulated spectrum on each pressure well reproduces the observed spectrum.

The result of the simulation and the resultant parameters such as p_A/p_B and the exchange rate constant from the inside of the pore to outside are shown in Fig. 8(a) and 8(b), respectively. The p_A/p_B value and the exchange rate constant increase linearly as pressure increases from 0.75 MPa to 6 MPa, indicating that the exchange of xenon is dominated by the density of xenon for bulk xenon more efficiency than that for

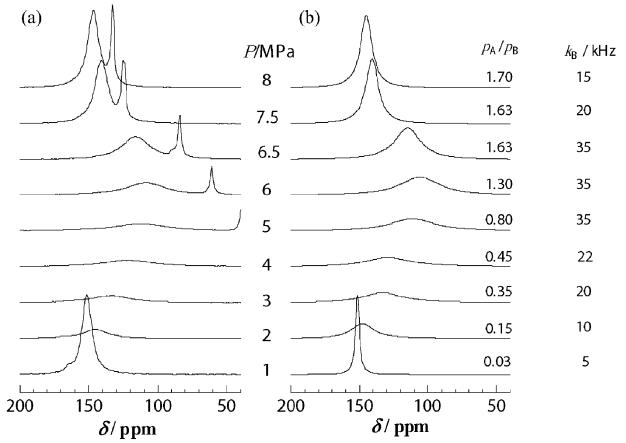

Fig. 7 Comparison of the observed spectra of xenon confined in NaY micropores and the simulated spectra, which are calculated on the basis of the two-site exchange model between the inside and outside of the micropores of NaY.

adsorbed xenon. Above 0.75 MPa, the pressure dependence of the chemical shift for adsorbed xenon seems to be saturated, and then the chemical exchange of xenon between the outside and the inside of the pores is accelerated by the increase in xenon density outside of the pores. In contrast, p_A/p_B seems to slightly increase above 6 MPa and the exchange rate constant decreases as pressure increases after the maximum at 6 MPa, where xenon outside the pores becomes supercritical fluid (T_c = 289.8 K and P_c = 5.8 MPa). This implies that under the supercritical fluid, a constant amount of xenon outside of the pores is concerned with the exchange of xenon inside of the pores. The origin of this behavior can not be clearly identified, but it may be concerned with the co-operative phenomenon in supercritical fluid such as the large fluctuation of xenon density and the large correlation length between xenon atoms.[62] The intermolecular coherence among xenon atoms in supercritical

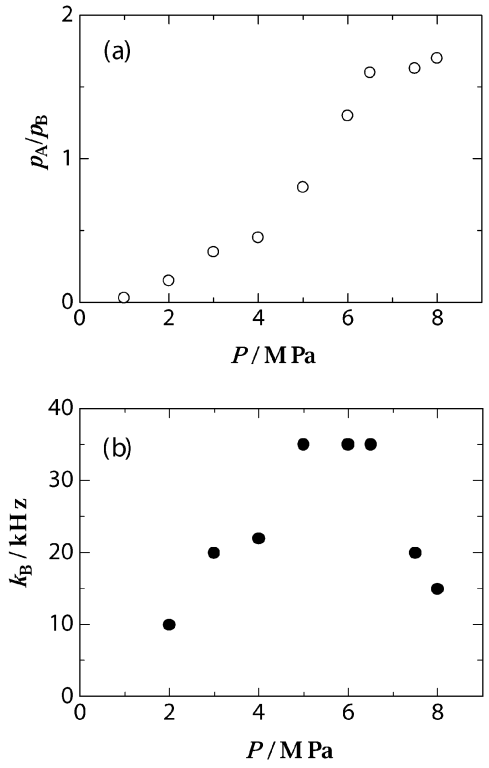

Fig. 8 Pressure dependence of the population ratio of free xenon to confined xenon, p_A(free Xe)/p_B(confined Xe) (a), and the exchange rate constant of xenon, k_B, between free xenon (outside of the micropore) and the confined one (inside of the micropore) (b).

fluid may promote the co-operative aggregation of xenon atoms such as the cluster formation.[63] This structure formation may contribute to decrease the efficiency of xenon exchange between the outside and inside of the pores.[64]

Finally, it is very interesting to show the different behavior of NaY on the chemical exchange from that of molecular sieve 13X, althought both zeolites have a same crystal structure. This different behavior on the chemical exchange will come from the difference in Si/Al values between X and Y type and/or the position of cations in the unit cell. In the present study, we can not examine what effect is dominant for the chemical exchange between the inside and the outside of the pore. The further study is now in progress.

5. Conclusion

In this study, high pressure ^{129}Xe NMR measurements were carried out to examine the local structure of confined xenon in the original micropores of the framework, as well as the effect of adsorbed water and the binding of polycrystalline on the xenon environments in molecular sieve 5A, 13X and zeolite NaY. The observations made were as follows:

1. The pressure dependence of the ^{129}Xe chemical shift value of xenon confined in the micropores of molecular sieve 5A, 13X and zeolite NaY are analyzed by the Langmuir adsorption model, leading to information about the pore size, the amount of xenon at saturated pressure, and the ratio of the apparent rate constant between the adsorption and desorption of xenon in the pores.

2. ^{129}Xe NMR spectrum and their pressure dependence enable us to detect decreases in the pore diameter due to the adsorption of water and the formation of additional micropores due to the binding of polycrystalline for pellet production. The super cage in molecular sieve 13X (FAU type framework) can accommodate water more efficiently than that in molecular sieve 5A (LTA type framework).

3. The analysis of the pore diameter assuming a spherical and the cylinder shaped pore suggests that the mobility of xenon adsorbed in the micropore of the framework increases in the order NaY > 13X > 5A. In zeolite NaY, the chemical exchange of xenon between the inside and outside of the micropore can be observed at high-pressure regions above 1 MPa.

4. The exchange rate constant and the population of xenon contributing to the exchange seem to be affected by the supercritical phenomena of bulk xenon gas co-existing with adsorbed xenon in the micropore. In the supercritical state, the exchange rate decreases, although the population of xenon in the micropores and the bulk gas is almost constant.

Thus, the high-pressure ^{129}Xe NMR technique offers new microscopic aspects on the pore structure, the intermolecular interaction of xenon confined in the pore, and the dynamical behavior of adsorbed xenon. This method will be a useful and powerful tool to investigate the porosity of materials from a microscopic point of view, and will be developed as a compensative method of the adsorption isotherm in the characterization of pore structure.

Acknowledgements

We thank Mr Takahiro Ueno of Takeda Chemical Industries, Ltd for his preliminary ^{129}Xe NMR measurements on molecular sieve 5A. This work was partially supported by a grant-in aid for Scientific Research (No. 11440176) from the Japanese Ministry of Education, Culture, Sports, Science and Technology.

References

1 E. G. Derouane, *A molecular view of heterogeneous catalysis: proceedings of the First Francqui Colloquium*, De Boeck Université, 1998.
2 K. Jacek, *Chem. Rev*., 1991, **91**, 1459.
3 P. B. Weisz and V. J. Frilette, *J. Phys. Chem*., 1960, **64**, 382.
4 I. Mochida, S. Hayato, A. Kato and T. Seiyama, *J. Catal*., 1971, **23**, 31.
5 T. Ito and J. Frassard, in *Proceedings of the 5th International Zeolite Conference, Naples*, ed. L. V. C. Rees, Heyden, London, 1980, p. 510.
6 P. J. Barrie and J. Klinowski, *Prog. NMR Spectrosc*., 1992, **24**, 91 and references therein.
7 D. Raftery and B. F. Chmelka, *NMR Basic Principles and Progress*, 1994, **30**, 112 and references therein.
8 J. Frassard, in *Encyclopedia of Nuclear Magnetic Resonance*, ed. M. Grant and R. Harris, John Wiley & Sons, Chichester, 1996, **vol. 5**, p. 3058.
9 C. I. Ratcliffe, *Annu. Rep. NMR Spectrosc*., 1998, **36**, 124, and references therein.
10 M.-A. Springuel-Huet, J.-L. Bonardet, A. Gédéon and J. Fraissard, *Magn. Reson. Chem*., 1999, **37**, S1, and references therein.
11 T. Koskela, M. Ylihautala and J. Jokisaari, *Microporous Mesoporous Mater*., 2001, **46**, 99.
12 J. M. Kneller, T. Pietrass, K. C. Ott and A. Labouriau, *Microporous Mesoporous Mater*., 2003, **62**, 121.
13 T. Koskela, J. Jokisaari and C. Satyanarayana, *Microporous Mesoporous Mater*., 2004, **67**, 113.
14 F. Chen, M. Zhang, Y. Han, F. Xiao, Y. Yue, C. Ye and F. Deng, *J. Phys. Chem. B*, 2004, **108**, 3728.
15 F. Chen, C.-L. Chen, S. Ding, Y. Yue, C. Ye and F. Deng, *Chem. Phys. Lett*., 2004, **383**, 309.
16 I. L. Moudrakovski, A. Sanchez, C. I. Ratcliffe and J. A. Ripmeester, *J. Phys. Chem. B*, 2000, **104**, 7306.
17 M. S. Syamala, R. J. Cross and M. Saunders, *J. Am. Chem. Soc*., 2002, **124**, 6216.
18 J. M. Kneller, R. J. Soto, S. E. Surber, J.-F. Colomer, A. Fonseca, J. B. Nagy, G. V. Tendeloo and T. Pietrass, *J. Am. Chem. Soc*., 2000, **122**, 10591.
19 A. P. M. Kentgens, H. A. van Boxtel, R.-J. Verweel and W. S. Veeman, *Macromolecules*, 1991, **24**, 3712.
20 M. Tomaselli, B. H. Meier, P. Robyr, U. W. Suter and R. R. Ernst, *Chem. Phys. Lett*., 1993, **205**, 145.
21 K. Sperling-Ischinsky and W. S. Veeman, *J. Braz. Chem. Soc*., 1999, **10**, 299.
22 B. Nagasaka, H. Omi, T. Eguchi, H. Nakayama and N. Nakamura, *Chem. Phys. Lett*., 2001, **340**, 473.
23 J. A. Ripmeester, C. I. Ratcliffe and J. S. Tse, *J. Chem. Soc. Faraday Trans*., 1988, **84**, 3731.
24 J. A. Ripmeester and C. I. Ratcliffe, *J. Phys. Chem*., 1990, **94**, 8773.
25 I. L. Moudrakovski, A. A. Sanchez, C. I. Ratcliffe and J. A. Ripmeester, *J. Phys. Chem. B*, 2001, **105**, 12338.
26 S. V. J. Torhaug, F. Liebig and C. R. Bowers, *J. Phys. Chem. B*, 2002, **106**, 2884.
27 O. Muenster, J. Jokisaari and P. Diehl, *Mol. Cryst. Liq. Cryst*., 1991, **206**, 179.
28 J. Bharatam and C. R. Bowers, *J. Phys. Chem. B*, 1999, **103**, 2510.
29 M. Ylihautala, J. Lounila and J. Jokisaari, *Chem. Phys. Lett*., 1999, **301**, 153.
30 A. Cherubini and A. Bifone, *Progr. NMR Spectrosc*., 2003, **42**, 1 and references therein.
31 E. Locci, Y. Dehouck, M. Casu, G. Saba, A. Lai, M. Luhumer, J. Reisse and K. Bartik, *J. Magn. Reson*., 2001, **150**, 167.
32 S. M. Rubin, M. M. Spence, A. Pines and D. E. Wemmer, *J. Magn. Reson*., 2001, **152**, 79.
33 T. Pietrass, *Magn. Reson. Rev*., 2000, **17**, 263 and references therein.
34 B. M. Goodson, *J. Magn. Reson*., 2002, **155**, 157.
35 B. Nagasaka, T. Eguchi, H. Nakayama, N. Nakamura and Y. Ito, *Radiat. Phys. Chem*., 2000, **58**, 581.
36 T. Ueda, T. Eguchi, N. Nakamura and R. E. Wasylishen, *J. Phys. Chem. B*, 2003, **107**, 180.
37 H. Kobayashi, T. Ueda, K. Miyakubo and T. Eguchi, *Z. Naturforsch., A*, 2003, **58a**, 727.
38 H. Omi, B. Nagasaka, K. Miyakubo, T. Ueda and T. Eguchi, *Phys. Chem. Chem. Phys*., 2004, **6**, 1299.
39 D. Baumer, A. Fink and E. Brunner, *Z. Phys. Chem*., 2003, **217**, 289.
40 T. B. Reed and D. W. Breck, *J. Am. Chem. Soc*., 1956, **78**, 5972.
41 K. Seff and D. P. Shoemaker, *Acta Cryst*., 1967, **22**, 162.
42 L. Broussard and D. P. Shoemaker, *J. Am. Chem. Soc*., 1960, **85**, 1041.
43 G. R. Eulenberger, D. P. Shoemaker and J. G. Keil, *J. Phys. Chem*., 1967, **71**, 1812.
44 K. S. W. Sing, D. H. Everett, R. A. W. Haul, L. Moscou and R. A. Pierotti, *Pure Appl. Chem*., 1985, **57**, 603.
45 K. Kaneko, *J. Membrane Sci*., 1994, **96**, 59.
46 J. H. deBoer, B. G. Linsen, Th. van der Plas and G. J. Zondervan, *J. Catal*., 1965, **4**, 649.
47 J. M. Thomas, C. A. Fyfe, S. Ramdas, J. Klinowski and G. C. Gobbi, *J. Phys. Chem*., 1982, **86**, 3061.
48 S. Ramdas and J. Klinowski, *Nature*, 1984, **308**, 521.
49 J. M. Thomas and J. Klinowski, *Adv. Catal*., 1985, **33**, 199.
50 A. D. H. Clague, *Helv. Phys. Acta*, 1985, **58**, 121.
51 A. J. Jameson, A. K. Jameson, R. E. Gerald II and H.-M. Lim, *J. Phys. Chem. B*, 1997, **101**, 8418.
52 J. Fraissard and T. Ito, *Zeolite*, 1988, **8**, 350, and references therein.
53 M. M. Dubinin, *Chem. Rev*., 1960, **60**, 235.
54 D. H. Everett and J. C. Poul, *J.Chem. Soc. Faraday Trans. 1*, 1976, **72**, 619.
55 Q. J. Chen and J. Frassard, *J. Phys. Chem*., 1988, **96**, 5170.
56 J. Demarquay and J. Fraissard, *Chem. Phys. Lett*., 1987, **136**, 314.
57 C. J. Jameson and D. Stueber, *J. Chem. Phys*., 2004, **120**, 10200, and references therein.
58 C. J. Jameson and A. C. de Dios, *J. Chem. Phys*., 1992, **97**, 417.
59 K. Kaneko, K. Shimizu and T. Suzuki, *J. Chem. Phys*., 1992 **97**, 8705.
60 J. Sandström, *Dynamic NMR Spectroscopy*, Academic Press, London, 1982.
61 S. A. Smith, T. O. Levante, B. H. Meier and R. R. Ernst, *J. Magn. Reson., Ser. A*, 1994, **106**, 75.
62 K. Nishikawa and T. Morita, *Chem. Phys. Lett*., 2000, **316**, 238.
63 O. Kajimoto, *Chem. Rev*., 1999, **99**, 355 and references therein.
64 H. Takaba, M. Katagiri, M. Kubo, R. Vetrivel, E. Broclawik and A. Miyamoto, *Surf. Sci*., 1996, **357–358**, 703.
65 R. M. Ruthven and R. I. Derrah, *Can. J. Chem. Eng*., 1972, **50**, 743.
66 A. Gedeon, T. Ito and J. P. Fraissard, *Zeolites*, 1988, **8**, 376.